Trans. Tianjin Univ. (2017) 23:501–510
DOI 10.1007/s12209-017-0065-y

RESEARCH ARTICLE

Performance of Methanol-to-Olefins Catalytic Reactions by the Addition of PEG in the Synthesis of SAPO-34

Yaquan Wang[1] · Zhao Wang[1] · Chao Sun[1] · Hengbao Chen[1] · Hongyao Li[1] · Haoyang Li[1]

Received: 27 June 2016 / Revised: 14 September 2016 / Accepted: 20 October 2016 / Published online: 20 June 2017

Abstract SAPO-34, a silicoaluminophosphate zeolite, has been synthesized by the hydrothermal method with the addition of different molecular weights of polyethylene glycol (PEG), and has been characterized with XRD, SEM, N_2 adsorption–desorption, FT-IR, and NH_3 temperature-programmed desorption (NH_3-TPD). We studied SAPO-34 as a catalyst in the methanol-to-olefins (MTO) reaction, in a fixed-bed reactor. The results show that the chain length of PEG has a great influence on the particle size and morphology of SAPO-34. PEG acts as inhibitor in the crystallization process. With the increase of the chain length of PEG used in the synthesis, from a relative molecular weight of 400–6000, the morphology of SAPO-34 changes gradually from cubic to nanoplate-like and then changes to cubic again. The particle size decreases markedly at first and then increases to some extent. The catalytic stability in the MTO reaction also increases first and then decreases, with all the catalysts having almost the same selectivity to olefins. When the sample is synthesized with PEG800, the particles become nanoplate-like with a thickness of 46 nm on average, and the catalytic stability is appreciably prolonged, which is attributed to the shorter diffusion paths of the reactants in the zeolite.

Keywords SAPO-34 · Polyethylene glycol · Chain length · Particle size · Nanoplate · Methanol-to-olefins

✉ Yaquan Wang
yqwang@tju.edu.cn

[1] Key Laboratory for Green Chemical Technology of the Ministry of Education, School of Chemical Engineering and Technology, Tianjin University, Tianjin 300072, China

Introduction

Zeolites with shape selectivity, high surface area, and high thermal stability, such as ZSM-5, TS-1, and SAPO-34 [1–7], are increasingly common in the field of catalysis, because microporous materials with selected properties and functions are in extreme demand in the contemporary chemical industry. SAPO-34, a silicoaluminophosphate zeolite with a large chabazite (CHA) framework structure and small 8-ring pore (0.38 nm × 0.38 nm), has attracted great attention as a catalyst in a number of reactions, such as hydrogen purification, CO_2/CH_4 separation, the dehydration of fructose into HMF, and the conversion of methanol-to-olefins (MTO) [8–11]. Among the reactions mentioned above, the MTO reaction plays an important role in the chemical energy industry. It has been shown that the MTO process is an extremely successful process for the production of light olefins, because it is a non-petrochemical route, and methanol is very inexpensive as a raw material. With the rapid rise of energy consumption, research of MTO and SAPO-34 is obviously necessary and urgent.

Since the Union Carbide Corporation invented SAPO molecular sieves in the 1980s [12], numerous experiments have been conducted to optimize the catalytic properties of SAPO-34 catalysts, including changing the materials and synthesis methods, such as the hydrothermal synthesis method and steam-assisted dry gel conversion method [13, 14]. Lee et al. [15] discovered that SAPO-34 synthesized with a mixture of both morpholine and tetraethyl ammonium hydroxide (TEAOH) as the template could reduce the particle size and lead to morphological changes compared with using a single template. Wang et al. [16] synthesized SAPO-34 crystallites with smaller crystallites (160 nm), larger surface areas (648 m^2/g), and more acid

sites than the catalysts synthesized with the traditional method via a two-step hydrothermal crystallization. Charghand et al. [17] used the ultrasound-assisted hydrothermal method and synthesized SAPO-34 with a higher surface area, perfect crystallinity, and uniform particle size. Álvaro-Muñoz et al. [18] shortened the crystallization time from days to several hours by using microwave-assisted hydrothermal synthesis and obtained nanocrystalline SAPO-34 catalysts. Yang et al. [19] obtained mesoporous SAPO-34 by introducing polyethylene glycol (PEG20000) as a mesogenerator during the synthesis process and tested the catalyst in the dehydration of fructose into HMF. Cui et al. [20] synthesized SAPO-34 with PEG2000 and obtained samples with a coarse and rough surface containing a large number of mesopores. Razavian and Fatemi [21] found almost the same result in their research and concluded that PEG could act as both a crystal growth inhibitor and mesogenerator, which depended on the synthesis condition. Xu et al. [22] reached a similar conclusion when synthesizing SAPO-34 and ZSM-5 small crystals with PEG as crystal growth inhibitor.

According to Guo et al. [23], wandering PEG polymer molecules surround the surface of preformed particles to postpone further growth. In addition, the chain length of PEG is capable of affecting the particle size and morphology. Much research has been carried out with PEG, but the effect of the polymerization degree of the PEG on the synthesis of SAPO-34 and the performance of SAPO-34 synthesized with different chain lengths of PEG in the MTO reaction have never been reported.

In this work, PEG with different polymerization degrees was introduced as a molecular sieve growth inhibitor during the hydrothermal synthesis of SAPO-34 catalysts. The addition of PEG with different polymerization degrees in the synthesis can reduce the particle size and change the morphology from cubic to nanoplate-like, which is in favor of the mass transfer in the MTO reaction. The effect of PEG on the textural properties of SAPO-34 catalysts is investigated by SEM, XRD, FT-IR, NH_3 temperature-programmed desorption (NH_3-TPD), and N_2 adsorption–desorption.

Experiment

Materials

Pseudoboehmite (58% Al_2O_3) was purchased from Shandong Aluminium Industry Co., Ltd., China. Phosphoric acid (85%), methanol (AR) and polyethylene glycol (PEG400, PEG800, PEG2000, and PEG6000) were purchased from Tianjin Guang Fu Fine Chemical Research Institute Co., Ltd., China. LUDOX As-40 colloidal silica (40 wt% suspension in water) was purchased from Sigma-Aldrich. TEAOH 35 (wt% aqueous solution) was purchased from Zhenjiang Runjing High Purity Chemical Co., Ltd., China.

Synthesis of SAPO-34

SAPO-34 crystals were prepared in the reaction mixtures with molar compositions of 1 Al_2O_3:0.2 SiO_2:1 P_2O_5:70 H_2O:2 TEAOH. In the synthesis of sample-400 to sample-6000, 5 g of various molecular weights of PEG (PEG400, PEG800, PEG2000 and PEG6000) was introduced into the above mixture. For the synthesis of sample-0, no PEG was added into the mixture. The preparation of SAPO-34 catalysts was conducted as described in Ref. [20]. In a typical preparation of sample-400, 5.79 g deionized water was mixed with 4.48 g pseudoboehmite first, and then 5.91 g phosphoric acid was added dropwise. After continuous stirring for 1 h, 0.77 g silica sol was added into the resultant solution slowly, and then stirred for 1 h continuously. Finally, 5 g PEG400 was introduced into the mixture. The reaction mixture was further stirred for 2 h, until a homogeneous mixture was obtained. Then the mixture was transferred into a Teflon-lined autoclave and aged at 120 °C for 24 h. Subsequently, the autoclave was heated at 200 °C for 48 h. The product was separated after the autoclave cooled down to room temperature, and washed with deionized water 3–4 times. Then the product was dried at 120 °C for 24 h, followed by calcination at 550 °C for 5 h at a heating rate of 2.5 °C/min. In order to exclude the effect of PEG concentration, different amounts of PEG 800 (0.67, 2, and 10 g) were introduced into the above mixture, synthesized and treated in the same way. The samples are designated as S–x–y, with x and y representing the molecular weight and the grams of PEG, respectively.

Characterization

XRD analysis was conducted on a Rigaku D/max 2500 diffractometer using a graphite monochromator with Cu Kα radiation ($\lambda = 0.15418$ nm) at a scanning rate of 8°/min from 5° to 40°. SEM images were obtained from an S-4800 field-emission scanning electron microscope with an accelerating voltage of 5 kV. FT-IR spectra of the catalysts were obtained by a Bruker Vertex 7.0 Fourier transform infrared spectrometer using the KBr technique. The infrared absorbance spectra were recorded from 4000 to 400 cm^{-1} with a resolution of 4 cm^{-1}. N_2 adsorption/desorption isotherms were measured on a Micromeritics Tristar 3000 apparatus at −196 °C. The specific surface areas were calculated by the Brunauer–Emmett–Teller (BET) equation, and the micropore surface areas and micropore volumes were calculated by a *t*-plot. The surface acidity of the catalyst was measured by NH_3-TPD on a Xianquan TP-5076 TPD analyzer equipped with a thermal conductivity detector. The heating rate was 10 °C/min.

Methanol-to-Olefins Reaction in a Fixed-Bed Reactor

A 1 g sample of SAPO-34 catalyst (20–40 mesh) mixed with 1 g quartz, of the same particle size, was added into a quartz tube reactor ($L = 320$ mm, $d = 12$ mm). The temperature of the reactor was maintained at 425 °C, and the temperature fluctuations during the reaction were kept less than 0.5 °C. The system was protected by a constant N_2 flow of 60 cm^3 min^{-1} to make the reactants flow through the catalysts at a particular flow rate and to protect the catalysts from reacting with air. A mixed solution of methanol and H_2O was fed into the reactor by a micropump. The molar ratio of methanol/H_2O was 1:1. In order to evaluate the life of the catalyst accurately, the weight hourly space velocity (WHSV) of the methanol was kept at 2 h^{-1} (2 g methanol per gram catalyst per hour), as per the industry standard.

Product Analysis

The products were analyzed by an online gas chromatograph, SP-2100, with a flame ionization detector and a packed-column KB-PLOT-Q (50 m × 0.32 mm × 10 μm) to separate the C_1–C_8 hydrocarbons. The temperature of the column was maintained at 60 °C for 4 min and then increased to 180 °C at a heating rate of 20 °C/min. C_2–C_3 were the main products and C_4–C_8 were the main byproducts. The conversion of methanol $X_{methanol}$ and the selectivity to C_2–C_3, $S_{C2–C3}$, were calculated as follows:

$$X_{\text{methanol}} = 1 - \frac{n_{\text{methanol}} + n_{\text{dimethylether}}}{n_{c_1} + 2n_{c_2} + 3n_{c_3} + 4n_{c_4} + 5n_{c_5} + 6n_{c_6} + 7n_{c_7} + 8n_{c_8}} \times 100\%, \quad (1)$$

and

$$S_{c_2-c_3} = \frac{2n_{\text{ethylene}} + 3n_{\text{propylene}}}{n_{c_1} + 2n_{c_2} + 3n_{c_3} + 4n_{c_4} + 5n_{c_5} + 6n_{c_6} + 7n_{c_7} + 8n_{c_8}} \times 100\%, \quad (2)$$

where n is the mole of the product detected by the online gas chromatograph.

Results and Discussion

Characterization of SAPO-34 Prepared with Different Molecular Weights of PEG

XRD patterns of the synthesized SAPO-34 are shown in Fig. 1, which clearly show the well-resolved peaks in the range of 5°–40°. It can be obviously observed that all the catalysts synthesized with or without PEG have the CHA structure of SAPO-34 at $2\theta = 9.5°$, 12.9°, 15.0°, 17.7°, 20.6°, 24.9°, 25.9°, 30.6°, and 31.0°, indicating that all the samples were successfully crystallized with a high degree of crystallinity and are related to SAPO-34 without any crystalline impurities, as reported in Refs. [24, 25]. In addition, the peak at 20.6° partly indicates the particle size of the sample [16]. From the height of the peak at 20.6° in the XRD patterns, we can see that the particle size becomes smaller when PEG was introduced. In addition, the S-800 samples (S-800-0.67, S-800-2, S-800-5, and S-800-10), which are synthesized with PEG800, exhibit the least intense reflection and have a relatively ill-defined pattern at the 20.6° peak, which suggests that the crystallite size of S-800 samples is significantly smaller than those of all the other samples. It can also be observed that the S-800 patterns are decreasing in peak intensity and are broadening; this change shows that the average particle size of the S-800 samples is around 200 nm [15, 16]. The relative crystallinity, calculated by comparing the total intensity of the five characteristic peaks of SAPO-34 at $2\theta = 9.5°$, 12.9°, 15.0°, 17.7°, and 20.6°, are listed in Table 1 [26]. The crystallinity of S-0 is taken as 100%. The results indicate that the relative crystallinity of SAPO-34 decreases with the addition of PEG. As the molecular weight of PEG increases from 400 to 800, the relative crystallinity of the samples decreases slightly. Subsequently, the relative crystallinity increases with increasing molecular weight of PEG from 800 to 6000. What causes the phenomenon is the addition of PEG that acted as a crystal growth inhibitor of SAPO-34 during the synthesis, because different molecular weights of PEG can hinder the crystal growth of the catalysts to different extents. However, the SAPO-34 samples synthesized with different amounts of PEG 800 have similar particle sizes and relative crystallinities.

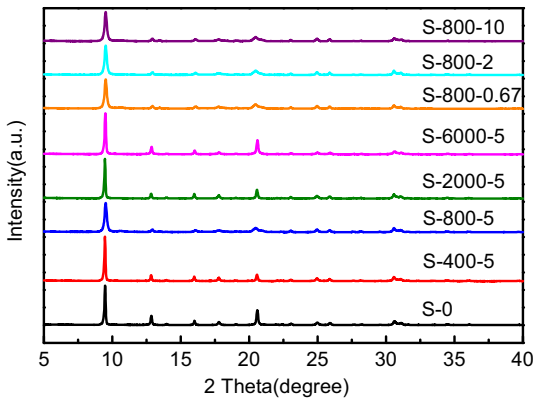

Fig. 1 XRD patterns of SAPO-34 synthesized with PEG

Table 1 Textural properties of SAPO-34 samples

Sample	Average particle size (nm)	Relative crystallinity (%)	S_{BET} (m^2/g)	S_{micro} (m^2/g)	S_{ext} (m^2/g)	V_{micro} (cm^3/g)
S-0	1931	100	592	582	10	0.268
S-400-5	467	88	609	586	23	0.274
S-800-5	267	84	626	580	46	0.271
S-2000-5	580	91	603	582	21	0.275
S-6000-5	1536	98	596	584	12	0.276
S-800-0.67	272	83	/	/	/	/
S-800-2	284	84	/	/	/	/
S-800-10	281	83	/	/	/	/

S_{BET} is BET surface area, S_{micro} is micropore surface area, S_{ext} is external surface area, V_{micro} is micropore volume

Figure 2 shows the SEM images of SAPO-34 catalysts synthesized with different molecular weights of PEG. It can be seen from the images that sample-0, which was synthesized without PEG, is a typical cube-like SAPO-34 with an average particle size of 1931 nm. With the addition of different molecular weights of PEG, the particle size and morphology of the catalysts change to some extent. The average particle size of each sample is listed in Table 1. It can be observed that the average particle sizes of SAPO-34 decrease with the increasing molecular weight of PEG from 400 to 800. However, as the molecular weight of PEG increases from 800 to 6000, the average particle sizes of the samples increase. The particles in the SEM images of S-400-5 and S-2000-5 almost have the same morphology. Most of the particles shown in the images of S-400-5 and S-2000-5 are not very cube-like. Some defects can be noticed easily on the surface of the cube. The reason for this phenomenon is inhibition during the crystallization process caused by the introduction of PEG. The SEM image of S-800-5 shows that all the crystals exhibit uniform nanoplate-like morphology, with an average particle size of 267 nm, which is in good agreement with the XRD results obtained above. Particularly, the thickness of each plate is thin and has an average particle size of 46 nm, which is in favor of mass transfer.

Figure 3 shows the SEM images of SAPO-34 catalysts synthesized with different amounts of PEG800. The SEM images show that all the samples synthesized with different amounts of PEG800 exhibit uniform nanoplate-like morphology. The average particle sizes of the samples are listed in Table 1. It can be concluded that the differences of the morphology and particle size among S-400-5 to S-6000-5 were not caused by the different amounts of added PEG.

In order to illustrate the formation mechanism of nanoplate-like SAPO-34, a schematic crystallization process is sketched in Scheme 1. To emphasize the effect of the growth inhibitor PEG, the formation mechanism of cube-like SAPO-34 is also sketched in Scheme 2 for comparison. As we can see in Scheme 2, the precursor solution partially crystalized to form disc-like particles at first. Secondly, the disc-like particles changed to be nanoplate-like with further crystal growth. Then the nanoplate-like crystals stacked one-by-one, and finally, the cube-like particle took shape [19, 27]. For the nanoplate-like sample, PEG was introduced into the precursor solution and existed in a chain-like state in it. When the nanoplate-like particles were formed, the chains of PEG adhered on the surface of the particles to form a protective film, which can protect the particles from stacking upon each other. Therefore, the length of the chain has a strong effect on the formation of the nanoplate [23]. If the chains are not long enough, the protective film, which is formed by the chains of PEG, would be too thin to prevent the particle from touching other particles. If the chains are too long, they are more likely to intertwine with each other and cannot adhere well to the surface of the particles or form a protective film.

The FT-IR spectra of SAPO-34 samples synthesized with different molecular weights of PEG are given in Fig. 4. The FT-IR spectra of all the samples are similar and agree with the typical FT-IR spectra of SAPO-34 reported in Ref. [28]. Framework vibrations can be observed at 490, 632, 730, 1095, 1651 and 3445 cm^{-1}, which are similar to those of the CHA structure [29]. The absorption peaks at 490 and 632 cm^{-1} are T–O bending bands of SiO_4 and D-6 rings, and the bands at 730 and 1095 cm^{-1} correspond to the symmetric stretch vibration of P–O and Al–O and asymmetric stretch vibration of O–P–O, respectively. Furthermore, the peak at 1651 cm^{-1} is the vibration of hydroxyl groups from adsorbed water on the samples. The last band at 3445 cm^{-1} is attributed to Si–OH and P–OH groups interacting through H-bonds [30].

The textural properties of the calcined catalysts were analyzed by nitrogen adsorption–desorption at −196 °C. The isotherms of SAPO-34 synthesized with different

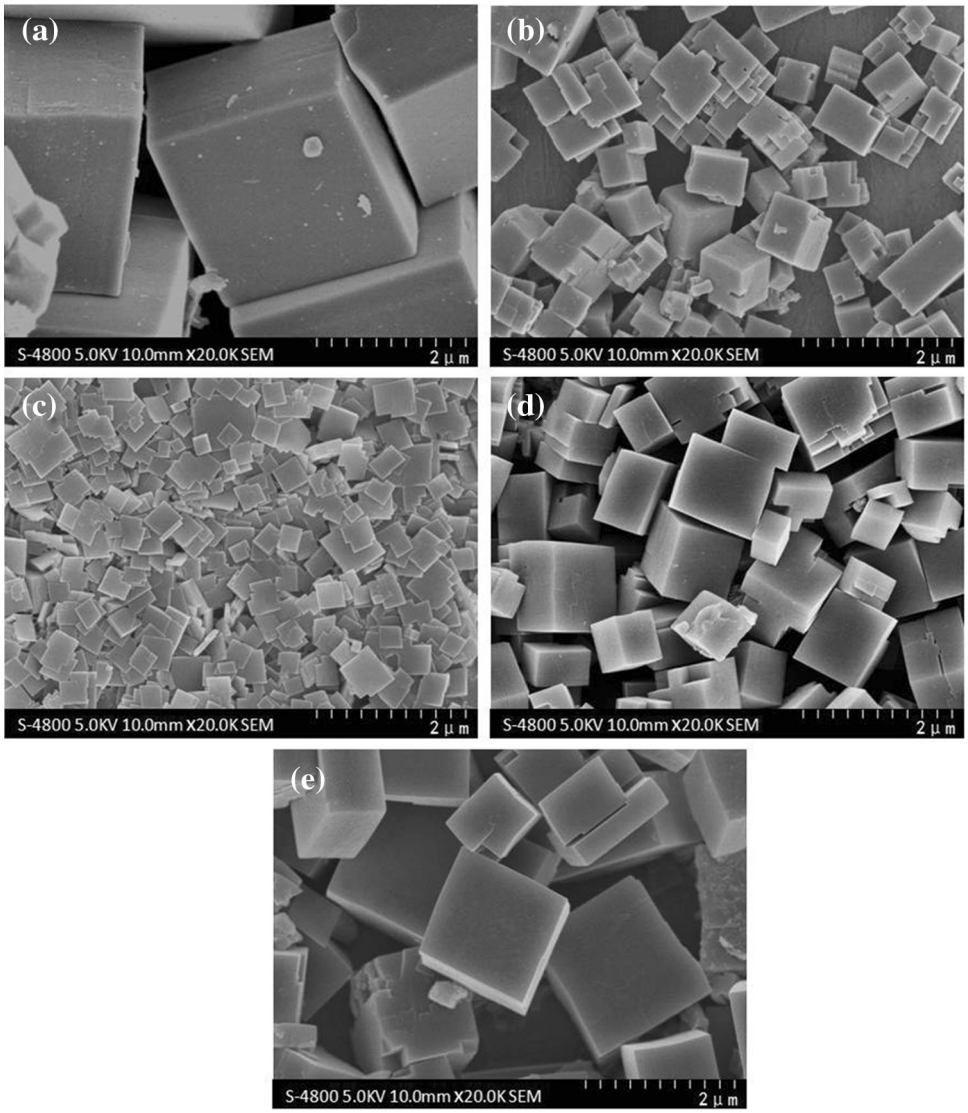

Fig. 2 SEM image of SAPO-34 synthesized with different molecular weights of PEG: **a** S-0, **b** S-400-5, **c** S-800-5, **d** S-2000-5, **e** S-6000-5

molecular weights of PEG are shown in Fig. 5. The BET specific surface areas, micropore surface areas, and micropore volumes of the samples are listed in Table 1. It can be observed that all the samples present type I isotherms according to the IUPAC classification [31, 32]. With the addition of PEG, the external surface area of the samples increased, but the micropore surface area almost have no change. This phenomenon is caused by the decrease of the particle size, which is shown in the SEM images. The additional nitrogen uptake and small hysteresis loop at high relative pressure in the isotherm of S-800-5 are caused by the interparticle spaces in the mesopore-size range [18]. It is necessary to mention that the technique used here is not the most appropriate method to detect the surface and pore volume of micropore materials, like SAPO-34, unambiguously. The results here should be used only for comparison [18].

NH_3-TPD was used to measure the acid properties of the samples. As shown in Fig. 6, two distinct NH_3 desorption peaks can be seen in the NH_3-TPD profiles at 180–220 °C and 400–500 °C. They are similar to the reported reference data for the acid properties of SAPO-34 [33]. Usually, the desorption temperature is a measure of the strength of the acid sites. The temperature desorption peaks at 180–220 °C are representative of the weak acid sites, which correspond to P–OH hydroxyl groups that are not fully coordinated by AlO_4 tetrahedra. The temperature desorption peaks at 400–500 °C are representative of the strong acid sites [34], which correspond to the incorporation of silicon into the framework of the SAPO-34 catalyst. The details of the concentrations of acid sites calculated by the areas of the temperature desorption peaks are shown in Table 2. It can be observed that the addition of PEG with different polymerization

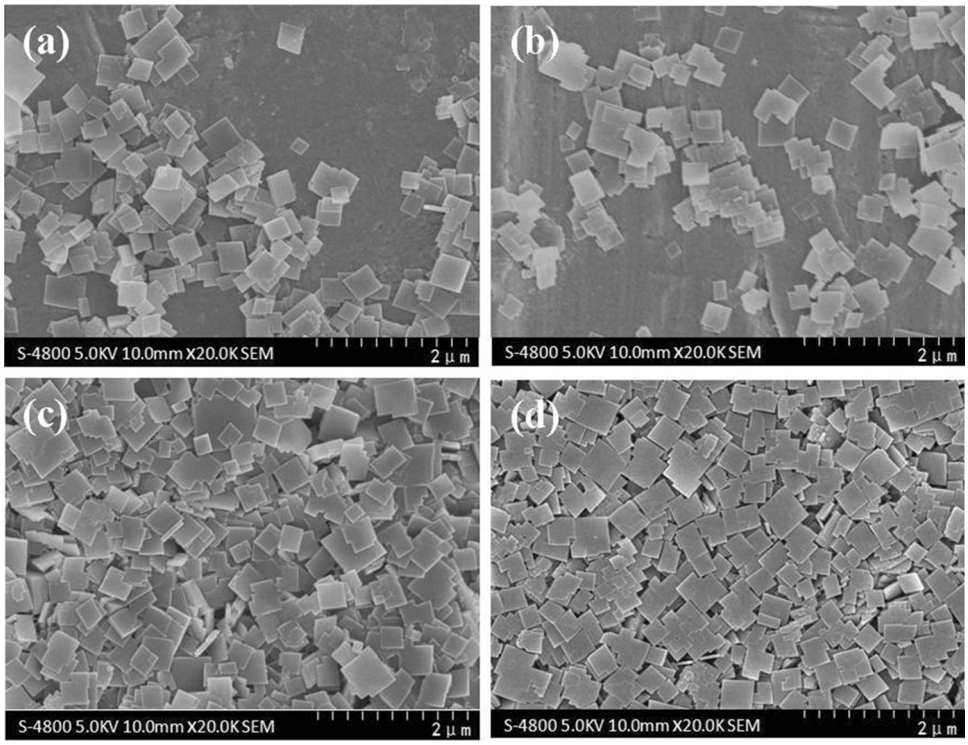

Fig. 3 SEM image of SAPO-34 synthesized with different amounts of PEG 800: **a** S-800-0.67, **b** S-800-2, **c** S-800-5, **d** S-800-10

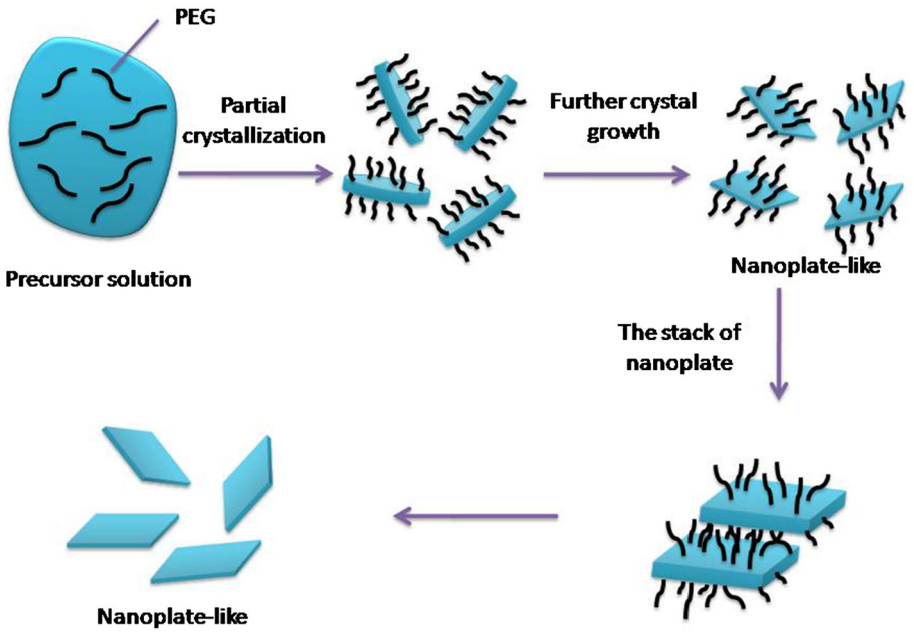

Scheme 1 Schematic representation of crystallization process of nanoplate-like SAPO-34 synthesized with TEAOH and PEG800

degrees has no systematic effect on the concentration of the weak acid sites. However, a slight decrease can be seen in the concentration of the strong acid sites with the addition of PEG, which is the same result that was reported in Ref. [31]. Therefore, the longer the chain of PEG is, the fewer strong acid sites will occur. As the strong acid site corresponds to the incorporation of silicon into the framework of SAPO-34 catalyst [35, 36], we can speculate that the long chain of PEG can hinder silicon from incorporating into the framework to some extent.

Catalytic Performance of SAPO-34 for the Methanol-to-Olefins Reaction

The catalytic performance of SAPO-34 synthesized with the addition of PEG in the methanol-to-olefins reaction

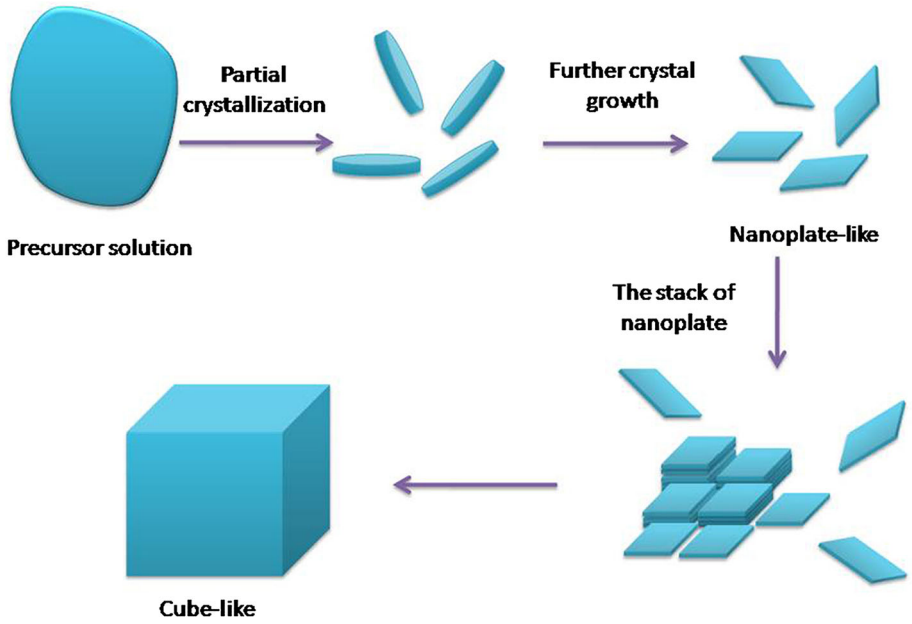

Scheme 2 Schematic representation of crystallization process of cube-like SAPO-34 synthesized with TEAOH

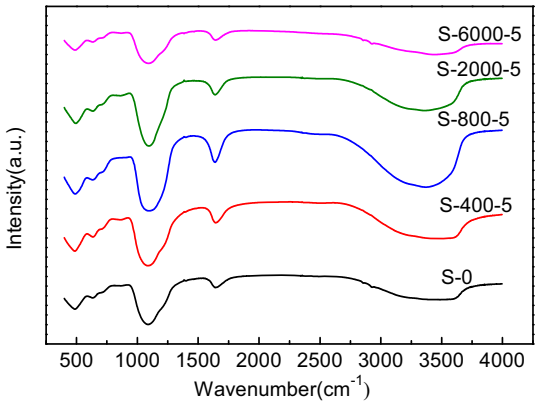

Fig. 4 FT-IR spectra of SAPO-34 synthesized with different molecular weights of PEG

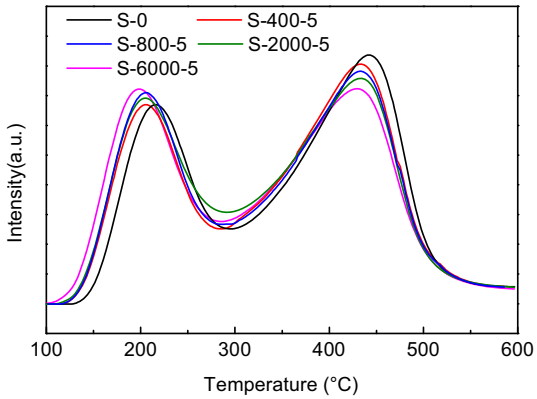

Fig. 6 NH_3-TPD profiles of SAPO-34 synthesized with different molecular weights of PEG

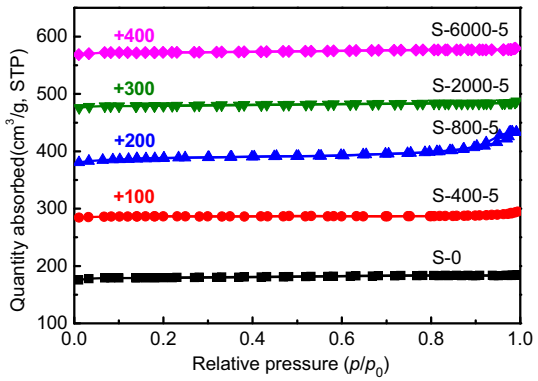

Fig. 5 N_2 adsorption–desorption isotherms of SAPO-34 synthesized with different molecular weights of PEG

Table 2 Acid properties of SAPO-34 samples

Sample	Weak acidity (mmol/g)	Strong acidity (mmol/g)	Total acidity (mmol/g)
S-0	0.59	0.70	1.29
S-400-5	0.58	0.67	1.25
S-800-5	0.65	0.66	1.31
S-2000-5	0.62	0.64	1.26
S-6000-5	0.66	0.62	1.28

has been investigated and the results are given in Fig. 7. All the samples show a high methanol conversion (100%) and high selectivity (80–86%) to ethylene and propylene during the stable online reaction time. The methanol

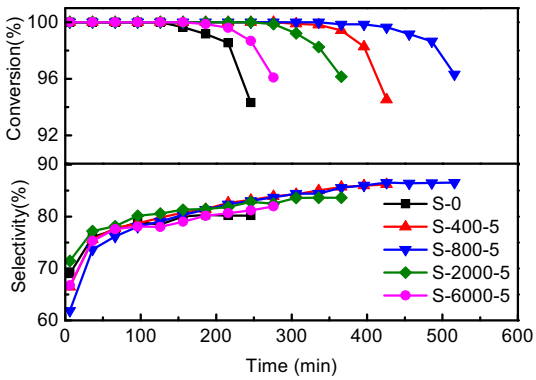

Fig. 7 Catalyst performance for the MTO reaction over SAPO-34 synthesized with different molecular weights of PEG (reaction conditions: $T = 425$ °C, $P = 1$ atm, 1.00 g catalyst mixed with 1 g quartz sand, 56.07 cm^3/min N_2, $CH_3OH:H_2O = 1:1$ (mol), WHSV (CH_3OH) = 2 h^{-1})

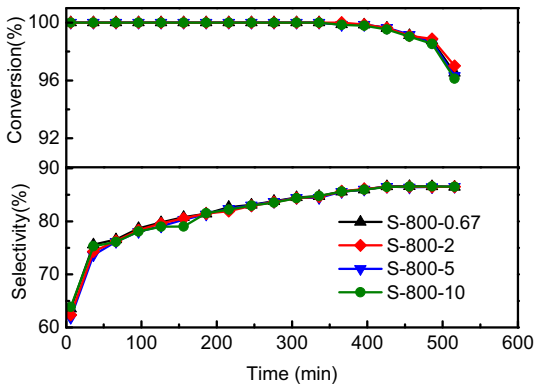

Fig. 8 Catalyst performance for the MTO reaction over SAPO-34 synthesized with different amounts of PEG800 (reaction conditions: $T = 425$ °C, $P = 1$ atm, 1.00 g catalyst mixed with 1 g quartz sand, 56.07 cm^3/min N_2, $CH_3OH:H_2O = 1:1$ (mol), WHSV (CH_3OH) = 2 h^{-1})

conversion over the SAPO-34 catalysts synthesized with PEG exhibits remarkably enhanced catalyst lifetimes, and the lifetimes of SAPO-34 synthesized with PEG400, PEG800, PEG2000, and PEG6000 are 306, 456, 366, and 216 min, respectively, which are much longer than 186 min for the conventional cube-like SAPO-34. The lifetime here represents the duration of time when the conversion of methanol is above 99%. Most likely, the changes in the performance of catalysts result from a combination of several effects: the particle size, the crystallinity, the concentration of strong acid sites, and the surface areas. Normally, SAPO-34 with a smaller concentration of strong acid sites exhibits slower catalyst deactivation and longer lifetimes. In contrast, a higher concentration is good for the conversion of methanol. This is why the sample synthesized without PEG has a higher selectivity than the other samples at the beginning of the reaction, but the sample synthesized without PEG exhibits a short lifetime. The reason could be that the bigger bulk crystal size of sample-0 leads to a longer diffusion path. With a longer diffusion path, the carbon chain of the products gets longer and longer with further conversion on the strong acid sites [37]. Finally, when the carbon chain is long enough to plug up the pore, the products inside the particles can no longer diffuse to the outside, which causes the fast carbon deposition and final deactivation [38]. In contrast, the nanoplate-like SAPO-34 with a smaller particle size, which is in favor of mass transfer, can greatly enhance the diffusion of the products inside the crystals, and thus inhibits the catalyst deactivation. As the reaction time continues, the carbon deposition makes the pores become smaller, and then long carbon chain products, like C_5 to C_8, have difficulty diffusing out of the particles, which is why the selectivity gets higher as the reaction time increases.

The catalytic performance of SAPO-34 synthesized with different amounts of PEG800 in the MTO process has been investigated and the results are given in Fig. 8. It can be observed that all the samples show excellent MTO performance. No appreciable difference could be seen on methanol conversion or selectivity among the samples. According to this result, it can be concluded that the differences on the MTO performance among S-400-5 to S-6000-5 were not caused by the different amounts of the added PEG.

Conclusions

SAPO-34 catalysts with different morphologies and particle sizes are synthesized by the hydrothermal method in which PEG acted as a crystal growth inhibitor. Compared with the traditional cube-like SAPO-34, the samples synthesized with PEG400 and PEG2000 are not very cube-like and have an obviously smaller particle size. Some defects could be noticed easily on the surface of the cube. The sample synthesized with PEG6000 has similar morphology with the traditional cube-like SAPO-34. But the average particle size, which is 1536 nm, is smaller than the typical one of 1931 nm. Nanoplate-like SAPO-34 with a thickness of 46 nm has been successfully synthesized with the addition of PEG800. PEG800 was charged into the synthesis to inhibit the intergrowth of the primary crystals via adherence to the surface of the primary crystal, thus, allowing the nanoplate-like catalyst to take shape.

An enhanced lifetime in the MTO reaction on the nanoplate-like catalyst was obtained. The prolonged lifetime has been attained without noticeable loss of selectivity. The strong acid sites and the improved mass transfer are the main causes of the prolonged catalytic lifetime of the nanoplate-like catalyst.

Acknowledgements This study was supported by the National Natural Science Foundation of China (No. 21276183).

References

1. Burton AW, Kliewer CE, Afeworki M (2015) Small crystal ZSM-5, its synthesis and use. Free Patents Online. 2001-01-30
2. Firoozi M, Baghalha M, Asadi M (2009) The effect of micro and nano particle sizes of H-ZSM-5 on the selectivity of MTP reaction. Catal Commun 10(12):1582–1585
3. Wu XX, Wang YQ, Zhang T et al (2014) Effect of TS-1 treatment by tetrapropyl ammonium hydroxide on cyclohexanone ammoximation. Catal Commun 50:59–62
4. Xu J, Wang YQ, Feng WP et al (2014) Effect of triethylamine treatment of titanium silicalite-1 on propylene epoxidation. Front Chem Sci Eng 8(4):478–487
5. Rostami RB, Ghavipour M, Behbahani RM et al (2014) Improvement of SAPO-34 performance in MTO reaction by utilizing mixed-template catalyst synthesis method. J Nat Gas Sci Eng 20:312–318
6. Álvaro-Muñoz T, Márquez-Álvarez C, Sastre E (2014) Aluminium chloride: a new aluminium source to prepare SAPO-34 catalysts with enhanced stability in the MTO process. Appl Catal A 472:72–79
7. Wang YQ, Ye JX, Wang SH et al (2016) Synthesis of mesoporous titanium silicalite-1 with high stability in cyclohexanone ammoximation. Trans Tianjin Univ 22(3):254–260
8. Golmakani A, Fatemi S, Tamnanloo J (2015) CO_2 capture from the tail gas of hydrogen purification unit by vacuum swing adsorption process, using SAPO-34. Ind Eng Chem Res 55(1):334–350
9. Iwase Y, Motokura K, Koyama TR et al (2009) Influence of Si distribution in framework of SAPO-34 and its particle size on propylene selectivity and production rate for conversion of ethylene to propylene. Phys Chem Chem Phys 11(40):9268–9277
10. Li SG, Falconer JL, Noble RD (2006) Improved SAPO-34 membranes for CO_2/CH_4 separations. Adv Mater 18(19):2601–2603
11. Salmasi M, Fatemi S, Najafabadi AT (2011) Improvement of light olefins selectivity and catalyst lifetime in MTO reaction; using Ni and Mg-modified SAPO-34 synthesized by combination of two templates. J Ind Eng Chem 17(4):755–761
12. Lok BM, Messina CA, Patton RL et al (1982) Silicoaluminophosphate molecular sieves: another new class of microporous crystalline inorganic solids. J Am Chem Soc 104(4):1146–1147
13. Fan D, Tian P, Xu ST et al (2012) A novel solvothermal approach to synthesize SAPO molecular sieves using organic amines as the solvent and template. J Mater Chem 22(14):6568–6574
14. Masoumi S, Towfighi J, Mohamadalizadeh A et al (2015) Tri-templates synthesis of SAPO-34 and its performance in MTO reaction by statistical design of experiments. Appl Catal A 493:103–111
15. Lee YJ, Baek SC, Jun KW (2007) Methanol conversion on SAPO-34 catalysts prepared by mixed template method. Appl Catal A 329:130–136
16. Wang PF, Yang DX, Hu J et al (2013) Synthesis of SAPO-34 with small and tunable crystallite size by two-step hydrothermal crystallization and its catalytic performance for MTO reaction. Catal Today 212:62.e61–62.e68
17. Charghand M, Haghighi M, Saedy S et al (2014) Efficient hydrothermal synthesis of nanostructured SAPO-34 using ultrasound energy: physicochemical characterization and catalytic performance toward methanol conversion to light olefins. Adv Powder Technol 25(6):1728–1736
18. Álvaro-Muñoz T, Sastre E, Márquez-Álvarez C (2014) Microwave-assisted synthesis of plate-like SAPO-34 nanocrystals with increased catalyst lifetime in the methanol-to-olefin reaction. Catal Sci Technol 4(12):4330–4339
19. Yang H, Liu XH, Guanzhong Lu et al (2016) Synthesis of SAPO-34 nanoplates via hydrothermal method. Microporous Mesoporous Mater 225:144–153
20. Cui Y, Zhang Q, He J et al (2013) Pore-structure-mediated hierarchical SAPO-34: facile synthesis, tunable nanostructure, and catalysis applications for the conversion of dimethyl ether into olefins. Particuology 11(4):468–474
21. Razavian M, Fatemi S (2014) Fabrication of SAPO-34 with tuned mesopore structure. Zeitschrift für anorganische und allgemeine Chemie 640(10):1855–1859
22. Xu F, Dong M, Gou WY et al (2012) Rapid tuning of ZSM-5 crystal size by using polyethylene glycol or colloidal silicalite-1 seed. Microporous Mesoporous Mater 163:192–200
23. Guo W, Luo GS, Wang YJ (2004) A new emulsion method to synthesize well-defined mesoporous particles. J Colloid Interface Sci 271(2):400–406
24. Aghaei E, Haghighi M (2014) Enhancement of catalytic lifetime of nanostructured SAPO-34 in conversion of biomethanol to light olefins. Microporous Mesoporous Mater 196:179–190
25. Xi DY, Sun QM, Xu J et al (2014) In situ growth-etching approach to the preparation of hierarchically macroporous zeolites with high MTO catalytic activity and selectivity. J Mater Chem A 2(42):17994–18004
26. Ma J, Si ZC, Wu XD et al (2016) Optimizing the crystallinity and acidity of H-SAPO-34 by fluoride for synthesizing Cu/SAPO-34 NH_3-SCR catalyst. J Environ Sci 41:244–251
27. Zheng JW, Zhang WP, Liu ZT et al (2016) Unraveling the non-classic crystallization of SAPO-34 in a dry gel system towards controlling meso-structure with the assistance of growth inhibitor: growth mechanism, hierarchical structure control and catalytic properties. Microporous Mesoporous Mater 225:74–87
28. Li Z, Martinez-Triguero J, Concepcion P et al (2013) Methanol to olefins: activity and stability of nanosized SAPO-34 molecular sieves and control of selectivity by silicon distribution. Phys Chem Chem Phys 15(35):14670–14680
29. Li JQ, Li Z, Han DZ et al (2014) Facile synthesis of SAPO-34 with small crystal size for conversion of methanol to olefins. Powder Technol 262:177–182
30. Li ZB, Martínez-Triguero J, Yu JH et al (2015) Conversion of methanol to olefins: stabilization of nanosized SAPO-34 by hydrothermal treatment. J Catal 329:379–388
31. Sun QM, Wang N, Guo GQ et al (2015) Synthesis of tri-level hierarchical SAPO-34 zeolite with intracrystalline micro–meso–macroporosity showing superior MTO performance. J Mater Chem A 3(39):19783–19789
32. Sun QM, Wang N, Xi DY et al (2014) Organosilane surfactant-directed synthesis of hierarchical porous SAPO-34 catalysts with excellent MTO performance. Chem Commun 50(49):6502–6505
33. Ye LP, Cao FH, Ying WY et al (2011) Effect of different TEAOH/DEA combinations on SAPO-34′s synthesis and catalytic performance. J Porous Mater 18(2):225–232

34. Wang PF, Lv AL, Hu J et al (2012) The synthesis of SAPO-34 with mixed template and its catalytic performance for methanol to olefins reaction. Microporous Mesoporous Mater 152:178–184
35. Wang C, Yang M, Tian P et al (2015) Dual template-directed synthesis of SAPO-34 nanosheet assemblies with improved stability in the methanol to olefins reaction. J Mater Chem A 3(10):5608–5616
36. Sastre G, Lewis DW (1998) Modelling of Brønsted acidity in AFI and CHA zeotypes. J Chem Soc Faraday Trans 94(19):3049–3058
37. Dai WL, Wang CM, Dyballa M et al (2015) Understanding the early stages of the methanol-to-olefin conversion on H-SAPO-34. ACS Catal 5:317–326
38. White JL (2011) Methanol-to-hydrocarbon chemistry: the carbon pool (r) evolution. Catal Sci Technol 1(9):1630–1635